Organically Templated Linear and Layered Iron Sulfates

Geo Paul, Amitava Choudhury, and C. N. R. Rao*

Chemistry and Physics of Materials Unit, Jawaharlal Nehru Centre for Advanced Scientific Research, Jakkur P.O., Bangalore 560 064, India

Received July 18, 2002. Revised Manuscript Received January 2, 2003

Linear and layered organically templated iron sulfates have been prepared under hydrothermal conditions. The linear iron sulfates, with the compositions $[H_3N(CH_2)_2NH_3][FeF_3(SO_4)]$, **I**, $[C(NH_2)_3]_2[FeF(SO_4)_2]$, **II**, $[H_3N(CH_2)_2NH_2(CH_2)_2NH_3][FeF(SO_4)_2]$, **III**, and $[H_2N(CH_2)_4NH_2][FeF_3SO_4]$, **IV**, possess the chain topologies found in tancoite, butlerite, and sideronatrite minerals. The layered sulfate **V**, with the composition $[H_3N(CH_2)_2NH_3][Fe_2F_2(SO_4)_2(H_2O)_2]$, can be considered to be formed from butlerite-type chains and with a structure similar to that of the layered fluorophosphate, ULM-10. Whereas the linear chains show the presence of antiferromagnetic interactions, the layered iron sulfate exhibits metamagnetism.

Introduction

Although the literature on open-framework inorganic materials is dominated by the families of alumino silicates[1] and phosphates,[2] there has been considerable effort to prepare other types of framework materials as well. Thus, several workers have prepared open-framework metal carboxylates.[3] Open-framework metal sulfates[4] and selenites[5] have also been reported in the literature. To prepare metal sulfates with open architecture, use of amine sulfates as starting materials has been suggested.[4,6] We have attempted to prepare open-framework iron sulfates by carrying out reactions of iron acetylacetonate with sulfuric acid in the presence of organic amines or directly by the reaction of the iron acetylacetonate with an amine sulfate under hydrothermal conditions. In this effort, we have obtained four organically templated linear chain sulfates: $[H_3N(CH_2)_2NH_3][FeF_3(SO_4)]$, **I**, $[C(NH_2)_3]_2[FeF(SO_4)_2]$, **II**, $[H_3N(CH_2)_2NH_2(CH_2)_2NH_3][FeF(SO_4)_2]$, **III**, and $[H_2N(CH_2)_4NH_2][FeF_3SO_4]$, **IV**. In addition, we have prepared a layered iron sulfate of the formula, $[H_3N(CH_2)_2NH_3][Fe_2F_2(SO_4)_2(H_2O)_2]$, **V**. To our knowledge, these compounds are some of the few members of the organically templated transition metal-sulfates. The linear chain sulfates show evidence for antiferromagnetic interactions, and the layered sulfate exhibits unusual magnetic properties involving ferromagnetic interactions as well. We believe that this success in preparing different types of amine-templated iron sulfates suggests that the sulfate ion can be used to build open-framework structures with novel magnetic and other properties.

Experimental Section

Synthesis and Initial Characterization. Compounds **I**−**V** were synthesized by employing mild hydro/solvothermal methods. In a typical synthesis, as in the case of **I**, 0.7113 g of $Fe(acac)_3$ was dissolved in an ethanol/H_2O mixture (5.8 mL/1.8 mL) under constant stirring. To this solution, was added 0.33 mL of H_2SO_4 (98%) and 0.42 mL of ethylenediamine (en). Finally, 0.3 mL of HF (48%) was added, and the mixture was stirred for 30 min to obtain a homogeneous gel. The final mixture with the molar composition of $Fe(acac)_3/H_2SO_4$/en/ethanol/H_2O/HF (1:3:3:50:50:3) was transferred into a 23-mL PTFE-lined acid digestion bomb and heated at 150 °C for 43 h. The product contained colorless needle-shaped crystals (with powder) that were monophasic (yield 90%). The various amines employed in **I**, **II**, and **III** are ethylenediamine (en), guanidine and diethylenetriamine (DETA), respectively. Compound **IV** was prepared by employing $[H_2N(CH_2)_4NH_2](SO_4)\cdot H_2O$ (PIPS) as the sulfate source. The piperazine sulfate, $[H_2N(CH_2)_4NH_2](SO_4)\cdot H_2O$ (PIPS), prepared following the procedure reported in the literature,[6] was reacted with $Fe(acac)_3$ under hydrothermal conditions. In the case of **V**, iron(III) citrate and ethylenediamine were employed for the synthesis. It is not clear whether the use of the citrate is responsible for obtaining **V**, as $Fe(acac)_3$ gives **I** with the same amine. It is, however, to be noted that in such kinetic controlled reactions carried out under hydro/solvothermal conditions, one obtains different products even with minor changes in reactions or reaction parameters. The introduction of fluoride ion is known to strongly influence the formation of the framework solids.[7,8] Details of the synthetic conditions for the preparation of the

* To whom correspondence should be addressed. E-mail: cnrrao@jncasr.ac.in.

(1) (a) Breck, D. W. *Zeolite Molecular Sieves*; Wiley: New York, 1974. (b) Meier, W. M.; Oslen, D. H.; Baerlocher, C. *Atlas of Zeolite Structure Types*; Elsevier: London, 1996.

(2) (a) Cheetham, A. K.; Férey, G.; Loiseau, T. *Angew. Chem., Int. Ed.* **1999**, *38*, 3268−3292. (b) Rao, C. N. R.; Natarajan, S.; Choudhury, A.; Neeraj, S.; Ayi, A. A. *Acc. Chem. Res.* **2001**, *34*, 80.

(3) (a) Li, H.; Eddaouidi, M.; O'Keeffe, M.; Yaghi, O. M. *Nature* **1999**, *402*, 276. (b) Serpaggi, F.; Ferey, G. *J. Mater. Chem.* **1998**, *8*, 2737. (c)Vaidhyanathan, R.; Natarajan, S.; Rao, C. N. R. *Chem. Mater.* **2001**, *13*, 185, and references therein.

(4) (a) Choudhury, A.; Jayaraman, K.; Rao, C. N. R. *Chem. Commun.* **2001**, 2610. (b) Paul, G.; Choudhury, A.; Rao, C. N. R. *J. Chem. Soc., Dalton Trans.* **2002**, 3859. (c) Paul, G.; Choudhury, A.; Rao, C. N. R. *Chem. Commun.* **2002**, 1904. (d) Paul, G.; Choudhury, A.; Sampathkumaran, E. V.; Rao, C. N. R. *Angew. Chem., Int. Ed.* **2002**, *41*, 4297.

(5) (a) Choudhury, A.; Udayakumar D.; Rao, C. N. R. *Angew. Chem., Int. Ed.* **2002**, *41*, 158, and references therein. (b) Harrison, W. T. A.; Phillips, M. L. F.; Stanchfield, J.; Nenoff, T. M. *Angew. Chem., Int. Ed.* **2000**, *39*, 3808.

(6) Jayaraman, K.; Choudhury, A.; Rao, C. N. R. *Solid State Sci.* **2002**, *4*, 413−422.

(7) (a) Guth, J. L.; Kessler, H.; Wey, R. *Stud. Surf. Sci. Catal.* **1986**, *28* 121. (b) Esterman, M.; McCusker, L. B.; Baerlocher, C.; Merrouche, A.; Kessler, H. *Nature (London)* **1991**, *352*, 320.

(8) Ferey, G. *J. Fluorine Chem.* **1995**, *72*, 187.

10.1021/cm020772p CCC: $25.00
Published on Web 02/15/2003

Table 1. Synthetic Conditions and Analyses for Compounds I−V

	starting composition[a]	*T* (K)	time (h)	pH[b]	Fe/S[c]	formula	yield %[d]
I	$Fe(acac)_3/H_2SO_4$/en/ethanol/H_2O/HF (1:3:3:50:50:3)	423	43	2 (3)	1:1	$[H_3N(CH_2)_2NH_3][FeF_3(SO_4)]$	90
II	$Fe(acac)_3/H_2SO_4$/GC[e]/butan-2-ol/EG[f]/H_2O/HF (2:3:1:50:50:50:6)	423	42	2 (2)	1:2	$[C(NH_2)_3]_2[FeF(SO_4)_2]$	25
III	$Fe(acac)_3/H_2SO_4$/DETA/EG/H_2O/HF (1:6:1.5:50:50:3)	423	144	2 (2)	1:2	$[H_3N(CH_2)_2NH_2(CH_2)_2NH_3]$ $[FeF(SO_4)_2]$	30
IV	$Fe(acac)_3$/PIPS/butan-2-ol/H_2O/HF (1:4:30:30:4)	423	48	2 (2)	1:1	$[H_2N(CH_2)_4NH_2][FeF_3SO_4]$	60
V	$Fe(ci)_3$[g]/H_2SO_4/en/butan-1-ol/H_2O/HF (1:3:3:25:50:6)	453	48	2 (2)	1:1	$[H_3N(CH_2)_2NH_3][Fe_2F_2(SO_4)_2(H_2O)_2]$	70

[a] The absolute quantities of iron complex taken are 0.7116 gm for **I**, 0.3558 gm for **II** and **III**, 0.1779 gm for **IV**, and 0.5260 gm for **V**. The H_2SO_4 used was 98% (w/w) in water, and HF used was 48% (w/w) in water. [b] The value in the parentheses indicates the final pH. [c] The ratios of the heavy elements were obtained from EDAX. [d] The yields were calculated with respect to iron. [e] Guanidine carbonate. [f] Ethylene glycol. [g] Iron(III) citrate.

various ironfluorosulfates are listed in Table 1. Compounds **I**−**V** were characterized by powder X-ray diffraction (XRD) and thermogravimetric analysis (TGA). Energy dispersive X-ray analysis (EDX) gave the expected Fe:S ratios. A chemical analysis and CHN elemental analysis was satisfactory indicating that fluorine contents are close to the stated values. Accordingly, the experimental and calculated (in wt %) elemental analysis of the chain structure **I** and the layered structure **V** are as follows: **I**, C, 8.93; N, 10.02; and H, 3.84; (calc.: C, 8.85; N, 10.30; H, 3.69); **V**, C, 5.32; N, 5.96; and H, 3.17; (calc.: C, 5.50; N, 6.40; H, 3.20).

Single-Crystal Structure Determination. Suitable single crystals of all the five compounds were carefully selected under a polarizing microscope and glued to a thin glass fiber with cyanoacrylate adhesive. Single-crystal data were collected on a Siemens SMART-CCD diffractometer [graphite-monochromated Mo kα radiation, $\lambda = 0.71073$ Å ($T = 298$ K)]. An absorption correction based on symmetry-equivalent reflections was applied using SADABS.[9] The structures were solved by direct methods using SHELXS-86[10] and difference Fourier synthesis. The direct methods solution readily revealed the heavy atom position (Fe and S) and enabled us to locate the other non-hydrogen positions (O, F, C, and N) from the Fourier difference maps. Fluorine and oxygen were located by making use of the Fourier difference maps and assigned by looking at the thermal parameters. Furthermore the Fe−F−Fe′ distances and angles are comparable to that of similar bonds reported earlier,[4c,d] but significantly different from the known Fe−O−Fe′ and Fe−(μ-OH)−Fe′ bond lengths reported in the literature. In the iron sulfate mineral network[11] the Fe^{3+}−(μ-OH)−Fe^{3+} bond distances are in the range 1.98−2.01 Å which are different from the Fe^{3+}−F−Fe^{3+} distances (in the range 1.871(2)−1.970(2) Å) and Fe^{2+}−F−Fe^{2+} distances (in the range 1.971(2)−2.057(6) Å) observed in **I**−**V**. The Fe−F−Fe′ distances, along with the results of the bond valence sum calculations and the absence of electron density near the fluorine in the difference Fourier map help to differentiate fluorine and hydroxyl groups. Hydrogen positions for the bonded [O(4) in **V**] as well as the extraframework amine molecules [**II**, **IV**, and **V**] were located from the difference Fourier map and placed in the observed position and refined isotropically. All the remaining hydrogen positions for **I** and **III** were initially located in the difference Fourier maps, and for the final refinement, the hydrogen atoms were placed geometrically and held in the riding mode. The last cycles of refinement included atomic positions for all the atoms, anisotropic thermal parameters for all non-hydrogen atoms, and isotropic thermal parameters for all the hydrogen atoms. Full-matrix least-squares structure refinement against $|F^2|$ was carried out using the SHELXTL-PLUS[12] package of programs. Details of the final refinements are given in Table 2. The powder X-ray diffraction patterns of all the five compounds were in good agreement with the simulated patterns generated from the single-crystal XRD data.

Results

$[H_3N(CH_2)_2NH_3][FeF_3(SO_4)]$, I. The asymmetric unit of **I** contains 13 non-hydrogen atoms of which 9 belong to the inorganic framework with one crystallographically distinct iron atom and one sulfur atom. The iron atom is octahedrally coordinated by O and F atoms to form an octahedron, and the S atom is presented as the SO_4 tetrahedron. The structure comprises strictly alternating octahedral FeF_3O_3 and tetrahedral SO_4 units, which form a four-member ring ladder (see Figure 1a). In the $[FeF_3(SO_4)]^{2-}$ ladder running along the *a*-axis, FeF_3O_3 octahedra share vertexes with triply bridging SO_4 groups. All the Fe−F bonds and the remaining S=O bond are terminal. The Fe−O bond distances are in the range 2.019(3)−2.042(3) Å, [$(Fe-O)_{av} = 2.031$ Å], and Fe−F the bond distances are in the range 1.871(2)−1.933(2) Å, [$(Fe-F)_{av} = 1.908(3)$ Å]. The *cis*-O/F−Fe−O/F bond angles are between 85.84(11) and 96.30(12)°, [(*cis*-O/F−Fe−O/F)$_{av}$ = 89.95(4)°] and the *trans*-O/F−Fe−O/F bond angles are between 173.22(10)−177.80(10)°, [(*trans*-O/F−Fe−O/F)$_{av}$ = 174.90(6)°]. The values of the bond distances and angles indicate that both Fe and S form near-perfect octahedron and tetrahedron, respectively. Bond valence sum (BVS)[13] calculations [Fe = 3.05, F(1) = 0.595, F(2) = 0.52, and F(3) = 0.503] indicate the valence state of Fe to be +3 and the positions of fluorine as terminal. The 1-D ladders along the *a*-axis in **I** are arranged parallel to one another in the *ab*-plane to form a layerlike arrangement shown in Figure 1(b). The layers are held together through hydrogen bonds by the diprotonated amine molecules located in the interlamellar space, to form the 3D assembly. The amine molecules interact with the framework oxygens and fluorines through N−H...O, N−H...F, and C−H...O hydrogen bonds to stabilize the structure.

$[C(NH_2)_3]_2[FeF(SO_4)_2]$, II. The asymmetric unit of **II** consists of 11 non-hydrogen atoms with one each of

(9) Sheldrick, G. M. SADABS: *Siemens Area Detector Absorption Correction Program*; University of Götingen: Götingen, Germany, 1994.

(10) (a) Sheldrick, G. M. SHELXS-86: *Program for Crystal Structure Determination*; University of Götingen: Germany, 1986. (b) Sheldrick, G. M. *Acta Crystallogr., Sect A* **1990**, *35*, 467.

(11) (a) Inami, T.; Nishiyama, M.; Maegawa, S.; Oka, Y. *Phys. Rev. B* **2000**, *61*, 12181. (b) Wills, A. S.; Harrison, A. *J. Chem. Soc., Faraday Trans.* **1996**, *92* (12), 2161. (c) Susse, P. *Z. Kristallogr.* **1972**, *135*, 34.

(12) Sheldrick, G. M. SHELXTL-PLUS *Program for Crystal Structure Solution and Refinement*; University of Götingen: Götingen, Germany.

(13) (a) Brese, N. E.; O'Keeffe, M. *Acta Crystallogr.* **1991**, *B47*, 192. (b) Brown, I. D.; Altermatt, D. *Acta Crystallogr.* **1985**, *B41*, 244.

Table 2. Crystal Data and Structure Refinement Parameters for I−V

structural parameter	I	II	III	IV	V
empirical formula	$[C_2N_2H_{10}][FeF_3(SO_4)]$	$[CN_3H_6]_2[FeF(SO_4)_2]$	$[C_4N_3H_{16}][FeF(SO_4)_2]$	$[C_4N_2H_{12}][FeF_3(SO_4)]$	$[C_2N_2H_{10}]_{0.5}[FeF(SO_4)(H_2O)]$
crystal system	orthorhombic	monoclinic	monoclinic	triclinic	triclinic
space group	$P2_12_12_1$	$C2/c$	$P2_1/c$	$P\bar{1}$	$P\bar{1}$
a (Å)	6.4111(6)	11.0508(9)	8.500(6)	7.3521(6)	5.0904(6)
b (Å)	9.5223(8)	16.0140(13)	7.305(6)	8.5698(6)	7.3687(9)
c (Å)	13.1307(12)	7.1023(5)	19.85(2)	8.5925(6)	9.1598(11)
α (°)	90	90	90	70.7840(10)	72.388(2)
β (°)	90	99.471(2)	96.49(4)	73.569(2)	85.257(2)
γ (°)	90	90	90	69.889(2)	71.025(2)
volume (Å)	801.61(12)	1239.7(2)	1224(2)	471.17(6)	309.97(6)
Z	4	8	4	2	2
formula mass	271.03	193.57	373.17	397.07	219.99
temperature (K)	298	298	298	298	298
ρ_{calc} (g cm^{-3})	2.246	2.074	2.024	2.904	2.357
μ (mm^{-1})	2.183	1.618	1.627	1.867	2.756
total data	3405	2589	4792	1991	1337
unique data	1146	893	1762	1328	886
data [$I > 2\sigma(I)$]	1057	770	806	1174	826
R_{int}	0.0343	0.0319	0.1171	0.0246	0.0328
R [$I > 2\sigma(I)$]	$R_1 = 0.0315$, $wR_2 = 0.0806$	$R_1 = 0.0284$, $wR_2 = 0.0689$	$R_1 = 0.0571$, $wR_2 = 0.1140$	$R_1 = 0.0315$, $wR_2 = 0.0814$	$R_1 = 0.0508$, $wR_2 = 0.1236$
	$R_1 = 0.0349$,[a] $wR_2 = 0.0825$[b]	$R_1 = 0.0370$,[a] $wR_2 = 0.0727$[b]	$R_1 = 0.1469$,[a] $wR_2 = 0.1474$[b]	$R_1 = 0.0346$,[a] $wR_2 = 0.0828$[b]	$R_1 = 0.0516$,[a] $wR_2 = 0.1243$[b]
goodness of fit (S)	1.054	1.098	0.913	1.009	1.072
no. of variables	119	117	175	188	123
largest difference map peak and hole e Å^{-3}	0.511 and −0.512	0.269 and −0.275	0.534 and −0.580	0.670 and −0.416	0.684 and −1.514

[a] $R_1 = \sum||F_o| - |F_c||/\sum|F_o|$. [b] $wR_2 = \{\sum[w(F_o^2 - F_c^2)^2]/\sum[w(F_o^2)^2]\}^{1/2}$, $w = 1/[\sigma^2(F_o)^2 + (aP)^2 + bP]$, $P = [F_o^2 + 2F_c^2]/3$; where $a = 0.0541$ and $b = 0$ for **I**; $a = 0.0341$ and $b = 1.3124$ for **II**; $a = 0.0520$ and $b = 0$ for **III**; $a = 0.0545$ and $b = 0$ for **IV**; $a = 0.0957$ and $b = 0$ for **V**.

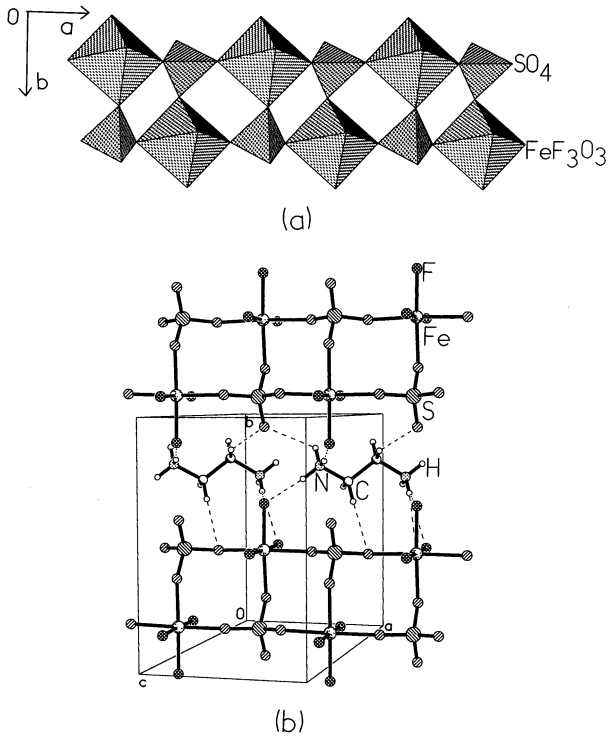

Figure 1. (a) Polyhedral view of **I**, showing the triply bridging sulfate tetrahedron and the alternating FeF_3O_3 octahedra and SO_4 tetrahedra. (b) Structure of **I** in the *ab*-plane. Note the orientations of amine molecules, and the interaction with the ladders. Dotted lines represent hydrogen bond interactions.

crystallographically distinct Fe and S. The structure is built up from seven framework atoms and contains FeF_2O_4 octahedra and SO_4 tetrahedra units. The Fe atoms make four Fe−O−S links and two Fe−F−Fe links to the nearby S atoms and Fe atoms, respectively. The

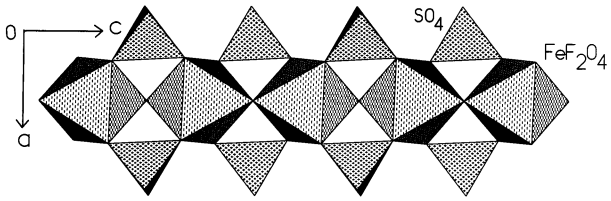

Figure 2. Polyhedral view of the inorganic part of **II**, along the *b*-axis with symmetrical bridging of the sulfate tetrahedra. Note the tancoite-type chains in **II**.

Fe octahedra share the axial fluorines with similar neighbors to produce a linear zigzag chain, and they share the equatorial oxygens with the SO_4 tetrahedra to form a tancoite[14] type topology. The SO_4 tetrahedra bridges pairs of Fe octahedra along the chain on both sides as shown in Figure 2. Two of the remaining SO_4 oxygens are terminal and are assigned as S═O bonds. This structure type is observed in open-framework metal phosphates[15] as well as in sulfate[16] and phosphate minerals.[14] The 1D chains in **II** are arranged parallel to one another in the *ab*-plane to form a layer like arrangement. Such layers are stacked one over the other along the *b* axis, with monoprotonated guanidine molecules residing in the interchain space. The guanidine cation hydrogen-bonded to the oxygens of the framework stabilizes the 3D assembly. The Fe−O bond distances are in the range 1.986(2)−2.012(2) Å with an average of 1.999 Å. The Fe−F bond distance is 1.9555(11) Å. The *cis*-O/F−Fe−O/F bond angles are between 87.50(9) and 92.50(9)°, [(*cis*-O/F−Fe−O/F)$_{av}$ = 90.0°] and the *trans*-

(14) Hawthrone, F. C. *Tschemaks Mineral. Petroger. Mitt.* **1983**, *31*, 121.
(15) Cavellec, M.; Riou, D.; Greneche, J. M.; Ferey, G. *Inorg. Chem.* **1997**, *36*, 2187.
(16) Hawthrone, F. C.; Krivovichev, S. V.; Burns, P. C. *Rev. Mineral. Geochem.* **2000**, *40*, 1.

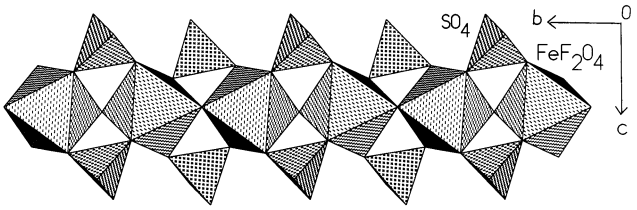

Figure 3. Polyhedral view of the inorganic part of **III**, along the *b*-axis. Note the structural similarity to **II**.

O/F−Fe−O/F bond angle is 180.0°. The values of the bond distances and angles indicate that both Fe and S form near-perfect octahedron and tetrahedron, respectively. BVS calculations [Fe = 3.03 and F(1) = 0.94] indicate the valence state of Fe to be +3 and the positions of the fluorine to be terminal.

$[H_3N(CH_2)_2NH_2(CH_2)_2NH_3][FeF(SO_4)_2]$, III. This iron sulfate is built up from 20 non-hydrogen atoms, of which 13 belong to inorganic framework and 7 belong to the guest molecules. There are two crystallographically distinct Fe atoms with both in the 2+ state and two S atoms. The framework is built up from the FeF_2O_4 octahedra and SO_4 tetrahedra. The structure of **III** (Figure 3) is similar to that of **II**, with the difference being in the templating amine. The triprotonated DETA molecule is hydrogen bonded to the framework oxygen and fluorine to stabilize the 3D crystalline assembly. BVS calculations [Fe(1) = 1.99, Fe(2) = 2.03] indicate the valence state of Fe to be +2 and confirm the positions of the fluorine ($F = 0.69$).

$[H_2N(CH_2)_4NH_2][FeF_3SO_4]$, IV. The asymmetric unit of **IV** consists of 16 non-hydrogen atoms, out of which 10 belong to inorganic framework and six belong to the organic guest molecules. There are two crystallographically distinct Fe atoms with octahedral geometry. The anionic framework $[FeF_3(SO_4)]^{2-}{}_n$ consists of FeF_4O_2 octahedra, sharing vertexes with similar neighbors through the fluorine. The sulfate tetrahedra are grafted onto the trans vertexes of the Fe octahedra along the chain. The trans orientation of the bridging F atom creates a zigzag {−F−Fe−F−Fe−} backbone to the linear chain of FeF_4O_2 octahedra, forming an analogue of the butlerite-type[17] chain (Figure 4a). In the sulfate tetrahedra, two oxygens bond to the adjacent Fe sites of the vertex-shared FeF_4O_2 octahedra in a symmetrical bridge, and the remaining two form terminal S=O bonds. The individual chains in **IV** are held together by hydrogen bond interactions involving diprotonated piperazine molecules. The arrangement of the amine molecules between the chains is such that different orientations of the amine molecule alternate as shown in Figure 4b. Hydrogen bond interactions involving the terminal S=O bond give rise to a sheet-like architecture possessing apertures, where the amine molecules reside. The 1D chains in **IV** also interact with the amine molecules via hydrogen bonds and form cavities. The cavities formed by such interactions (Figure 4b) resemble those in the organic porous structures formed through noncovalent interactions.[18] BVS calculations [Fe(1) = 3.03, Fe(2) = 3.09] indicate that the valence state of Fe is +3 and confirm the positions of the fluorine atom (F(1) = 0.57, F(2) = 0.92, and F(3) = 0.56).

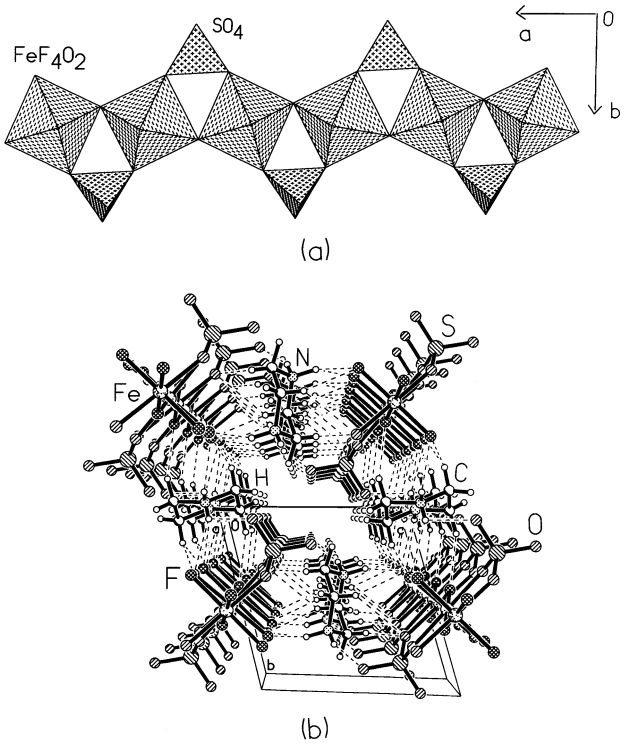

Figure 4. (a) Polyhedral view of the inorganic part of **IV**, along the *c*-axis with alternating up−down bridging of sulfate tetrahedron. Note the butlerite-type chains. (b) 3D assembly formed by the chains and the amine molecules in **IV**, creating a channel.

$[H_3N(CH_2)_2NH_3][Fe_2F_2(SO_4)_2(H_2O)_2]$, V. Of the 11 asymmetric non-hydrogen atoms in **V** nine belong to the inorganic framework and two are guests. The framework of the structure is built up from FeF_2O_4, $FeF_2O_2(H_2O)_2$ octahedra, and SO_4 tetrahedra, sharing vertexes, as Fe−F−Fe bonds and Fe−O−S bonds, the $Fe-OH_2$ bonds being terminal. The FeF_2O_4 and $FeF_2O_2(H_2O)_2$ octahedra are alternatively connected by their *trans*-fluorine vertexes and form an infinite chain, of {F−Fe−F−Fe−} backbone. The chains are connected to one another by the SO_4 tetrahedra, in such a way that each $FeF_2O_2(H_2O)_2$ octahedron is linked to two SO_4 groups and each FeF_2O_4 octahedron is linked to four SO_4 groups to produce the porous layer containing an eight-ring window (Figure 5a). The lamellar structure bears resemblance to the ironfluorophosphate reported by Ferey et al.[19] The structure of the 1D chains in this layer is similar to **IV** and is related to the topology of the mineral butlerite. The ethylenediamine cations occupy interlayer sites and are bound to the ironfluorosulfate layer through N−H...O hydrogen bonds as shown in Figure 5b. All the six N−H protons are involved in such linkages with oxygen atoms. The hydrogen bonds between the amines and the inorganic sheets ensure the stability of the structure.

The Fe−O bond distances in **V** are in the range 2.168(3)−2.188(4) Å with an average of Fe(1) = 2.1735 and Fe(2) = 2.183 Å. The Fe−F bond distances are in the range 1.971(2)−2.005(2) Å with an average of Fe(1)

(17) Fafani, L.; Nunzi, A.; Zanazzi, P. F. *Am. Mineral.* **1971**, *56*, 751.

(18) Ranganathan, A.; Pedireddi, V. R.; Rao, C. N. R. *J. Am. Chem. Soc.* **1999**, *120*, 1752.

(19) Cavellec, M.; Riou, D.; Ferey, G. *J. Solid State Chem.* **1994**, *112*, 441.

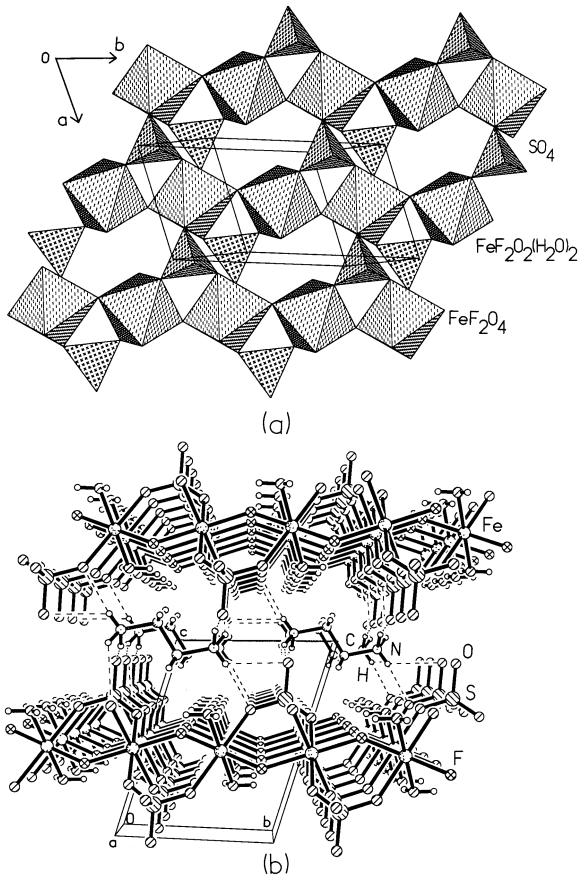

Figure 5. (a) Polyhedral view of the layer in **V**, showing the presence of butlerite-type chains fused together to create an eight-ring window. (b) View down the crystallographic *a*-axis showing the packing of layers in **V**. Note all the hydrogen in the nitrogen atom of amine molecule take part in hydrogen bonding.

= 2.005 and Fe(2) = 1.971 Å. The *cis*-O/F−Fe−O/F bond angles are between 83.73(11) and 96.27(11)°, [(*cis*-O/F−Fe(1)−O/F)$_{av}$ = 90.0° and (*cis*-O/F−Fe(2)−O/F)$_{av}$ = 90.0°] and the *trans*-O/F−Fe−O/F bond angle is 180.0°, indicating near-perfect octahedral geometry for Fe. The observed Fe−F/O bond distances, as well as BVS calculations [Fe(1) = 1.986 and Fe(2) = 2.027], indicate the valence state of both Fe(1) and Fe(2) to be 2+. The position of the bridging fluorine is supported by BVS calculations [F = 0.802]. Selected values of the bond distances and angles in **V** are listed in Table 3.

Magnetic Properties. One-dimensional homometallic magnetic systems can be antiferromagnetic or ferromagnetic depending on the sign of the nearest-neighbor exchange interactions.[20] Ferrimagnetism in chains is found when there is noncompensation of the spin moments.[21] At high temperatures, compounds **I**−**III** are paramagnetic and obey the Curie−Weiss law (Figure 6). The paramagnetic Curie temperatures are negative with values in the range of −38 to −46 K (−38 K for **I**, −41 K for **II**, and −46 K for **III**) indicating antiferromagnetic interactions.

Magnetic susceptibility measurements of the layered iron sulfate **V** reveal a complex behavior. High-temperature susceptibility data give a negative paramagnetic Curie temperature of −95 K. The plot of magnetic

Table 3. Selected Bond Distances (in Angstroms) and Angles (in Degrees) for $[C_2N_2H_{10}]_{0.5}[FeF(SO_4)(H_2O)]$, V[a]

moiety	distance	moiety	distance
Fe(1)−F(1)	2.005(2)	Fe(2)−O(3)^2	2.178(3)
Fe(1)−F(1)^1	2.005(2)	Fe(2)−O(4)^2	2.188(4)
Fe(1)−O(1)^1	2.168(3)	Fe(2)−O(4)	2.188(4)
Fe(1)−O(1)^1	2.168(3)	S(1)−O(1)	1.463(3)
Fe(1)−O(2)^1	2.179(3)	S(1)−O(2)^3	1.468(3)
Fe(1)−O(2)	2.179(3)	S(1)−O(5)	1.478(3)
Fe(2)−F(1)^2	1.971(2)	S(1)−O(3)^4	1.485(3)
Fe(2)−F(1)	1.971(2)	O(2)−S(1)^3	1.468(3)
Fe(2)−O(3)	2.178(3)	O(3)−S(1)^5	1.485(3)

moiety	angle	moiety	angle
F(1)−Fe(1)−F(1)^1	180	F(1)−Fe(2)−O(4)^2	88.6(2)
F(1)−Fe(1)−O(1)^1	96.27(11)	O(3)−Fe(2)−O(4)^2	86.46(14)
F(1)^1−Fe(1)−O(1)^1	83.73(11)	O(3)^2−Fe(2)−O(4)^2	93.54(14)
F(1)−Fe(1)−O(1)	83.73(11)	F(1)^2−Fe(2)−O(4)	88.6(2)
F(1)^1−Fe(1)−O(1)	96.27(11)	F(1)−Fe(2)−O(4)	91.4(2)
O(1)^1−Fe(1)−O(1)	180	O(3)−Fe(2)−O(4)	93.54(14)
F(1)^1−Fe(1)−O(2)^1	92.40(12)	O(3)^2−Fe(2)−O(4)	86.46(14)
F(1)^1−Fe(1)−O(2)^1	87.60(12)	O(4)^2−Fe(2)−O(4)	179.999(1)
O(1)^1−Fe(1)−O(2)^1	93.27(12)	O(1)−S(1)−O(2)	110.9(2)
O(1)−Fe(1)−O(2)^1	86.73(12)	O(1)−S(1)−O(5)	110.7(2)
F(1)−Fe(1)−O(2)	87.60(12)	O(2)^3−S(1)−O(5)	107.9(2)
F(1)^1−Fe(1)−O(2)	92.39(12)	O(1)−S(1)−O(3)^4	110.8(2)
O(1)^1−Fe(1)−O(2)	86.73(12)	O(2)^3−S(1)−O(3)^4	108.9(2)
O(1)−Fe(1)−O(2)	93.27(12)	O(5)−S(1)−O(3)^4	107.6(2)
O(2)^1−Fe(1)−O(2)	180	Fe(2)−F(1)−Fe(1)	135.79(13)
F(1)^2−Fe(2)−F(1)	180	S(1)−O(1)−Fe(1)	136.6(2)
F(1)^2−Fe(2)−O(3)	92.02(11)	S(1)^3−O(2)−Fe(1)	133.8(2)
F(1)−Fe(2)−O(3)	87.98(11)	S(1)^5−O(3)−Fe(2)	142.8(2)
F(1)^2−Fe(2)−O(3)^2	87.98(11)		
F(1)^2−Fe(2)−O(3)^2	92.02(11)		
O(3)−Fe(2)−O(3)^2	180		
F(1)^2−Fe(2)−O(4)^2	91.4(2)		

Organic Moiety

moiety	distance	moiety	distance
C(1)−N(1)	1.481(7)	N(1)−C(1)−C(1)^6	110.4(6)
C(1)−C(1)^6	1.487(11)		

[a] Symmetry transformations used to generate equivalent atoms: $^1-x+1, -y, -z+1$; $^2-x+1, -y+1, -z+1$; $^3-x, -y, -z+1$; $^4-x, -y-1, -z$; $^5x, y+1, z$; $^6-x+1, -y, -z+2$.

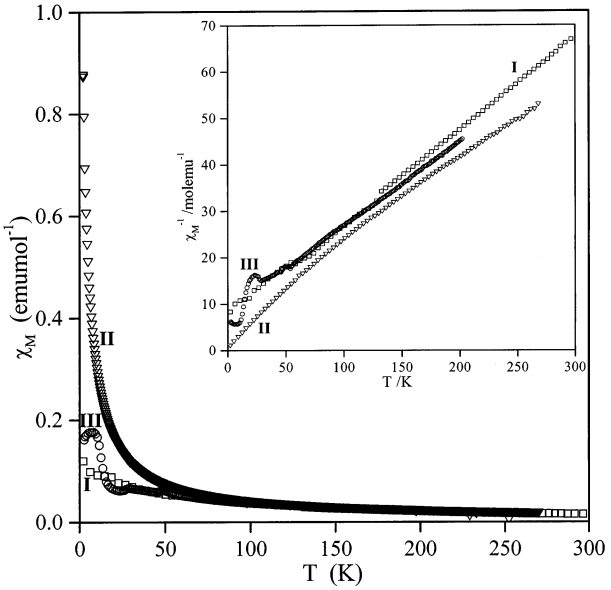

Figure 6. Temperature variation of the magnetic susceptibility for compounds **I**−**III**. Inset shows the variation of inverse susceptibility.

(20) (a) Kahn, O. *Molecular Magnetism*; VCH: New York, 1993; Chapter 11. (b) Day, P. *J. Chem. Soc., Dalton Trans.* **1997**, 701.

(21) Abu-Youssef, M. A. M.; Escuer, A.; Goher, Md., A. S.; Mautner, F. A.; Reib, G. J.; Vicente, R. *Angew. Chem., Int. Ed.* **2000**, *39*, 1624.

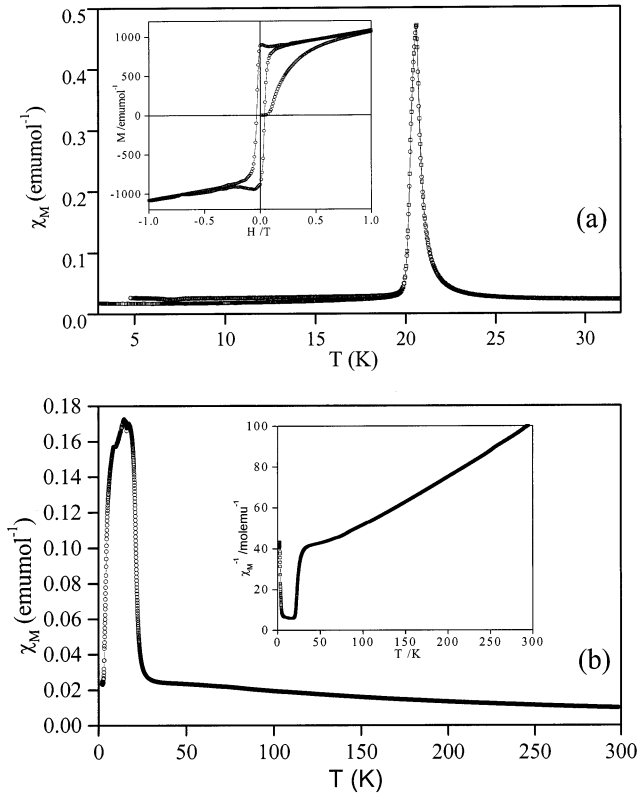

Figure 7. (a) DC magnetic susceptibility data of **V** showing the magnetic transition at 22 K and the nondivergence between the ZFC and FC data (at 100 Oe). Shown in the inset is hysteresis-loop at 10 K. (b) Temperature variation of χ_M and $\chi_M - 1$(inset) for compound **V**.

susceptibility (measured at 100 Oe) against temperature shows a sharp magnetic transition around 22 K (Figure 7a). The field-cooled (FC) and zero field-cooled (ZFC) data are superimposable showing thereby that the 22 K transition is not due to a frustrated system such as a spin-glass. The transition appears to be due to competing ferromagnetic and antiferromagnetic interactions. Thus, **V** shows magnetic hysteresis at 10 K, on an initial application of a small magnetic field (<0.1 T) as can be seen from the inset of Figure 7a. The sharp jump of magnetization at ~0.02 T is an indication of metamagnetism. Susceptibility measurements at a high field of 5 KOe (see Figure 7b) show a peak around 20 K somewhat like a ferrimagnet. It would be worthwhile to study the magnetic structure of **V** further to understand its properties.

Thermal Behavior. TGA curves (N_2 atmosphere, range 30−850 °C, heating rate 5 °C/min) of **I**−**V** given in Figure 8 show distinct mass losses. In **I** there is a two-step weight loss corresponding to the loss of the amine, HF and F_2 in the range 280−400 °C [obs = 43.9%, calc = 42.1%], and SO_3 at 500 °C [obs = 28.2%, calc = 29.5%]. **II** shows a gradual weight loss in the 300−600 °C range corresponding to the loss of guanidine, HF, and SO_3 [obs = 65.8%, calc = 67.2%]. In **III**, there is a sharp two-step weight loss corresponding to the loss of amine, HF, water, and SO_3 in the range 280−520 °C [obs = 78.8%, calc = 79%]. The TGA curve of **IV** reveals a three-step weight loss, of the amine at 315 °C [obs = 30.7%, calc = 29%], of HF at 390 °C [obs = 14.5%, calc = 13.5%], and of SO_3 at 480 °C [obs = 28.8%, calc = 27%]. In **V** there is a two-step weight loss corresponding to the loss of the amine, HF, and H_2O in the 180−400 °C range [obs = 31.1%, calc = 30.9%], and of SO_3 at 500 °C [obs = 34%, calc = 36%]. The powder X-ray diffraction patterns (PXRD) of the decomposed samples for **I** to **V** were characteristic of Fe_2O_3.

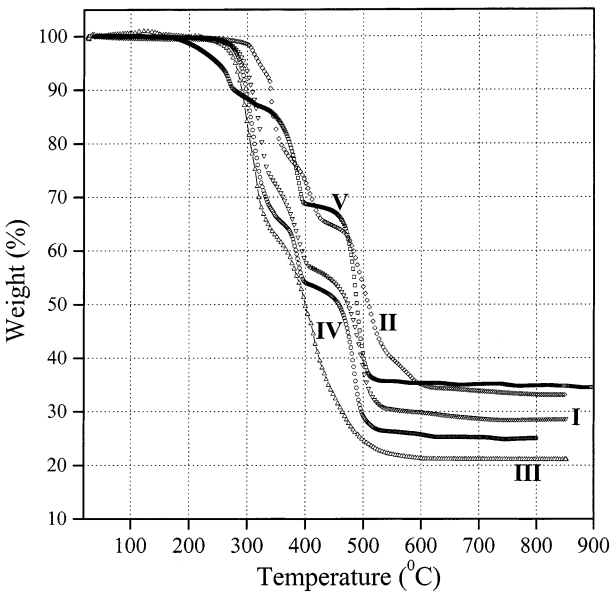

Figure 8. TGA curves of compounds **I**−**V**.

Discussion

The present study contributes five members to a new family of organically templated transition-metal sulfates. There are several noteworthy features in the structures reported here. Thus, **I** represents the first octahedral−tetrahedral (O−T) ladder in the metal-sulfate family. To our knowledge, there is only one report of an O−T ladder in the literature,[22] although a number of T−T ladders are known.[23] Because 1D ladders have been considered to be building units of higher dimensional structures,[26] the synthesis of the new ladder sulfate, **I**, is significant. The transformation of the T−T ladders to 2D and 3D structures in zinc phosphates has been examined in detail.[23a] An iron arsenate oxalate ladder is also reported to transform to 2D and 3D structures upon hydrothermal treatment.[22] There are, however, no dangling sulfate groups attached to the metal center in **I**, unlike in the ladder phosphates.[22,23]

As mentioned earlier, the topology of **II** and **III** occurs in some of the sulfate minerals as well as in a few other open-framework solids. Thus, the structures of sideronatrite, $Na_2[Fe^{3+}(OH)(SO_4)_2](H_2O)_3$, and metesideronatrite, $Na_4[Fe^{3+}{}_2(OH)_2(SO_4)_4](H_2O)_3$, are based on this topology,[16] as is also the structure of phosphate mineral

(22) Chakrabarti, S.; Natarajan, S. *Angew. Chem., Int. Ed.* **2002**, *41*, 1224.

(23) (a) Choudhury, A.; Neeraj, S.; Natarajan, S.; Rao, C. N. R. *J. Mater. Chem.* **2001**, *11*, 1537. (b) Bu, X.; Gier, T. E.; Stutkey, G. D. *Chem. Commun.* **1997**, 2271. (c) Harrison, W. T. A.; Bircsak, Z.; Hannooman, L.; Zhang, Z. *J. Solid State Chem.* **1998**, *136*, 93. (d) Williams, I. D.; Yu, J.; Gao, Q.; Chen, J.; Xu, R. *Chem. Commun.* **1997**, 1273. (e) Neeraj, S.; Natarajan, S.; Rao, C. N. R. *Angew. Chem., Int. Ed.* **1999**, *38*, 3880. (f) Neeraj, S.; Natarajan, S.; Rao, C. N. R. *Chem. Mater.* **1999**, *11*, 1390. (g) Choudhury, A.; Natarajan, S. *J. Mater. Chem.* **1999**, *9*, 3113. (h) Yan, W.; Yu, J.; Shi, Z.; Xu, R. *Inorg. Chem.* **2001**, *40*, 379.

tancoite, $Na_2LiH[Al(PO_4)_2(OH)]$. Synthetic variants of the tancoite chain in phosphate based materials have been encountered in systems of Al,[24] Ga,[25] and also Fe.[15,26] Two-iron phosphates with a similar topology have been reported recently in the literature.[27] Many synthetic 2D and 3D phosphates contain the tancoite type chain motif.[28] Clearly, the tancoite chain is one of the fundamental building units in open-framework materials based on MO_6 and TO_4 polyhedra. This has been realized in the GaPO-system where a tancoite-type chain is found to transform to 2D and 3D structures upon mild hydrothermal treatment.[29,30] Even though the oxidation states of iron in **II** and **III** are different, both form sideronatrite (or tancoite) type chains. In the sideronatrite chain, the charge balancing cation is Na^+ and the bridging moiety is OH, whereas in **II** and **III** they are the diprotonated amine and fluorine, respectively. **III** is probably the first example of a sideronatrite type chain with iron in the 2+ state.

The $[M(T\phi_4)\phi_3]$ chain in **IV** forms the basic motif in butlerite $[Fe^{3+}(OH)(H_2O)_2(SO_4)]$, parabutlerite $[Fe^{3+}(OH)(H_2O)(SO_4)]$, and uklonskovite $Na[MgF(H_2O)_2(SO_4)]$.[16] In this type of chain, tetrahedra alternate along the chain and link to the trans-vertexes of the octahedra. A similar chain of cis-corner-sharing octahedra (decorated with tetrahedra) occurs in fibroferrite, $[Fe^{3+}(OH)(H_2O)_2(SO_4)](H_2O)_3$. In butlerite, parabutlerite, and fibroferrite the chains are linked solely by hydrogen bonds, as there are no interstitial cations. In **IV**, however, the chains are held together by the hydrogen-bonded assembly of the diprotonated piperazine molecules located in the interchain space to form the 3D assembly. To our knowledge, there is no report on butlerite-type chains in the phosphate family.

The structure of **V** is similar to that of the iron fluorophosphate structure (ULM-10) reported by Ferey et al.,[19] which consists of infinite chains of alternating corner-sharing $Fe^{3+}F_2O_4$ and $Fe^{2+}F_2O_2(H_2O)_2$ octahedra decorated by PO_4 tetrahedra fused together to form the layered structure. ULM-11 and the mineral curetonite, $Ba_2[(Al,Ti)Al(PO_4)_2(OH,O_2)F]$, possess similar structures, being built up of the 'laueite' motif.[31] There are differences between the above compounds and **V** despite the similar topology of the inorganic part of the structures. In **V**, all the Fe atoms are in the 2+ state, and the atoms bridging the octahedral sites are fluorines. In **V**, charge balancing is done by the diprotonated amine (in ULM-10, monoprotonated en; ULM-11, metal-bonded en; curetonite, Ba^{2+}). Jacobson et al.[32] have reported two niobium phosphates and one titanium phosphate which are structurally similar to **V**. The butlerite-type chains in **IV** are fused together to form the layer architecture of **V**. This suggests that the butlerite chain in **IV** could be an intermediate in the formation of **V**.

Conclusions

Five organically templated iron sulfates have been synthesized under hydrothermal conditions, of which four possess 1D-chain structures and one has layered structure. The layered compound exhibits a complex magnetic behavior, which requires further study. The success in the synthesis of these iron sulfates suggests that the sulfate tetrahedron can be effectively used as a building unit to design open-framework inorganic solids. Such an effort is likely to lead to novel organically templated three-dimensional open-framework metal sulfates, which are not known to date.

Supporting Information Available: Tables of bond distances and angles, and hydrogen bonding interactions for the studied compounds, supplementary figures (PDF), and an X-ray crystallographic file (CIF) for **I**−**V**. These materials are available free of charge via the Internet at http://pubs.acs.org.

CM020772P

(24) (a) Attfield, M. P.; Morris, R. E.; Burshtin, I.; Campana, C. F.; Cheetham, A. K. *J. Solid State Chem.* **1995**, *118*, 412. (b) Lii, K. H.; Wang, S. L. *J. Solid State Chem.* **1997**, *128*, 21.

(25) (a) Lin, H. M.; Lii, K. H. *Inorg. Chem.* **1998**, *37*, 4220. (b) Walton, R. I.; Millange, F.; O'Hare, D.; Paulet, C.; Lossieau, T.; Ferey, G. *Chem. Mater.* **2000**, *12*, 1979. (c) Bonhomme, F.; Thoma, S. G.; Nenoff, T. M. *J. Mater. Chem.* **2001**, *11*, 2559.

(26) Cavellec, M.; Riou, D.; Ferey, G. *Inorg. Chem. Acta* **1999**, *291*, 317.

(27) (a) Choudhury, A.; Rao, C. N. R. *Zh. Struct. Khim.* **2002**, *43*, 681. (b) Mahesh, S.; Green, M. A.; Natarajan, S. *J. Solid State Chem.* **2002**, *165*, 334.

(28) (a) Lii, K. H.; Huang, Y. F. *Chem. Commun.* **1997**, 1311. (b) Moore, P. B.; Araki, T. *Am. Mineral.* **1974**, *59*, 964. (c) Moore, P. B.; Araki, T. *Am. Mineral.* **1977**, *62*, 692.

(29) Livage, C.; Millange, F.; Walton, R. I.; Loiseau, T.; Simon, N.; O'Hare, D.; Ferey, G. *Chem. Commun.* **2001**, 994.

(30) Walton, R. I.; Millange, F.; Bail, A. L.; Loiseau, T.; Serre, C.; O'Hare, D.; Ferey, G. *Chem. Commun.* **2000**, 203.

(31) (a) Cavellec, M.; Riou, D.; Ferey, G. *Eur. J. Solid State Inorg. Chem.* **1995**, *32*, 271. (b) Cooper, M.; Hawthorne, F. C. *Am. Mineral.* **1994**, *79*, 545.

(32) Wang, X.; Liu, L.; Cheng, H.; Rass, K.; Jacobson, A. J. *J. Mater. Chem.* **2000**, *10*, 1203.